# ORGANIC CHEMISTRY

## FRONTIERS

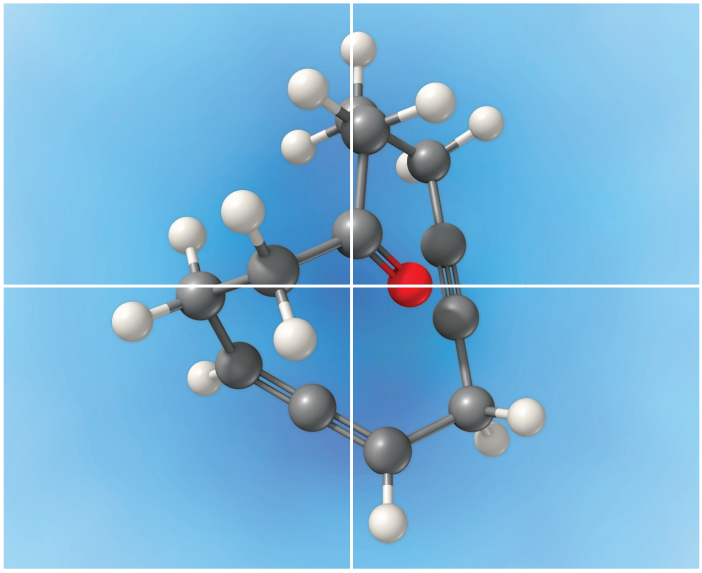

Accepted Manuscript

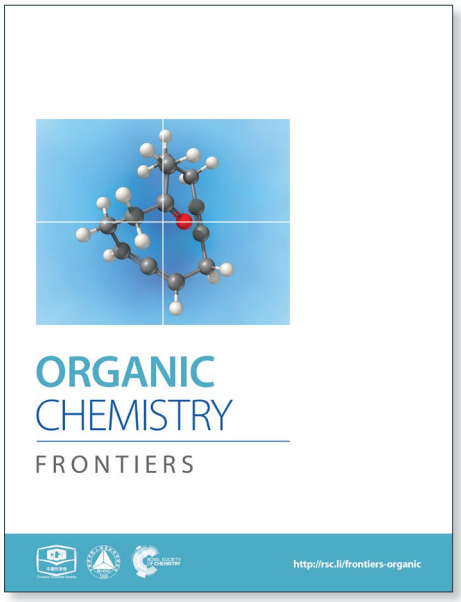


This is an *Accepted Manuscript*, which has been through the Royal Society of Chemistry peer review process and has been accepted for publication.

*Accepted Manuscripts* are published online shortly after acceptance, before technical editing, formatting and proof reading. Using this free service, authors can make their results available to the community, in citable form, before we publish the edited article. We will replace this *Accepted Manuscript* with the edited and formatted *Advance Article* as soon as it is available.

You can find more information about *Accepted Manuscripts* in the **Information for Authors**.

Please note that technical editing may introduce minor changes to the text and/or graphics, which may alter content. The journal's standard **Terms & Conditions** and the **Ethical guidelines** still apply. In no event shall the Royal Society of Chemistry be held responsible for any errors or omissions in this *Accepted Manuscript* or any consequences arising from the use of any information it contains.

Journal Name

ARTICLE

# Mechanism, Chemoselectivity and Enantioselectivity for Rhodium-Catalyzed Desymmetric Synthesis of Hydrobenzofurans: A Theoretical Study

Received 00th January 20xx,
Accepted 00th January 20xx

DOI: 10.1039/x0xx00000x

www.rsc.org/

Zhaoyuan Yu, Xiaotian Qi, Yingzi Li, Song Liu and Yu Lan*

Rhodium-catalyzed desymmetrization of cyclohexadienones is an efficient method for the asymmetric synthesis of hydrobenzofurans. The newly reported density functional theory (DFT) method MN12-L is used to investigate the mechanism, chemoselectivity and enantioselectivity for this type reactions. Computational results indicate that the preferred pathway involves transmetallation to form an aryl-rhodium compound, alkyne insertion, intramolecular olefin insertion, and protonation to generate the hydrobenzofurans product. The enantioselectivity is controlled by the intramolecular olefin insertion step, which is ascribed to the steric repulsions between ligand and substrate. In addition, the generation of side product via a second intermolecular alkyne insertion has also been considered in calculation.

## Introduction

As the structural core in numerous biologically important natural products, chiral *cis*-hydrobenzofurans are considered to be attractive targets for synthetic chemists.[1] Chiral organocatalysts catalyzed intramolecular desymmetrization of cyclohexadienones[2] is proven to be a usefull approach for the synthesis of *cis*-hydrobenzofurans derivates, such as Rauhut–Currier reaction[3] and Stetter reaction.[4] Besides, transition-metal catalysis have also emerged as a versatile and powerful tool among various synthetic methods.[5,6] In the presence of transition-metals, new carbon–carbon bonds can be formed easily via the unsaturated bond insertion into metal–carbon bond.[7] However, how to control the regio- and enantioselectivity in this type of insertion still remains a big challenge. More experimental[8] and theoretical investigations[9] require to be done to reveal the origin of selectivity.

Recently, rhodium-catalyzed asymmetric desymmetrization[10] of cyclohexadienones were reported by Lautens[11] group and Lin group,[12] which provided a useful methodology for the synthesis of functionalized hydrobenzofurans. As shown in Scheme 1, the reaction between cyclohexadienone-tethered alkyne **1** and arylboronic acid **2** using a rhodium(I)-catalyst,can afford *cis*-hydrobenzofuran **3** in yield up to 76%.[11] When 3,4-dimethoxy-phenyl derivative diene ligand is added, an enantioselective product can be formed with up to 88% enantiometric excess (*ee*). In some cases, side product **4** is also observed with about 19% yield. Almost at the same time, Lin reported a similar process for the rhodium-catalyzed synthesis of hydrobenzofurans.[12] The chiral bisphosphine ligand (*R*)-BINAP has numerous unique features, exhibit extremely high chiral recognition ability in catalytic reaction.[13] When the (R)-BINAP was employed, afford an enantioselective product hydrobenzofuurans in 99% yield and 99% *ee*.

Plausible mechanism for this rhodium-catalyzed synthesis of hydrobenzofurans was individually proposed by Lautens and Lin, however, the generation of chemoselectivity and enantioselectivity are still unclear. Density functional theory (DFT) calculations were thereby performed to reveal the mechanism, chemoselectivity, enantioselectivity, and the ligand effect of this type reaction.

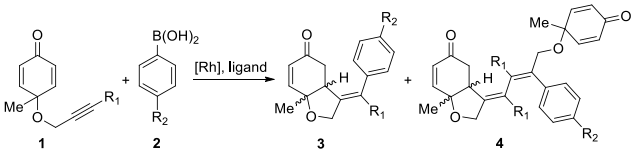


**Scheme 1** The Rhodium-Catalyzed Symmetric Desymmetrization of Cyclohexadienones.

## Computational methods

All the DFT calculations were carried out with the GAUSSIAN 09 series of programs.[14] The B3LYP[15] functional with the standard 6-31G(d) basis set[16] (LanL2DZ basis set[17] for rhodium atom) was used for the geometry optimizations. Harmonic frequency calculations were performed for all stationary points to confirm whether they were local minima or transition states and to derive the thermochemical corrections for the enthalpies and free energies. The MN12-L functional,[18] recently proposed by the Truhlar group, which could give more accurate energetic information, was used to calculate the single-point energies. The solvent effects were considered by single-point

*School of Chemistry and Chemical Engineering, Chongqing University, Chongqing 400044, P. R. China.*
*E-mail: lanyu@cqu.edu.cn*
Electronic Supplementary Information (ESI) available: [the calculated Cartesian coordinates and energies of all reported structures are available in supporting information]. See DOI: 10.1039/x0xx00000x

calculations of the gas-phase stationary points with SMD solvation model.[19] The larger basis set 6-311+G(d,p)[20] (LANL08 basis set[21] for rhodium atom) was used in the solvation single-point calculations. The energies given in this paper are the MN12-L calculated Gibbs free energies in methanol solvent.

## Results and discussion

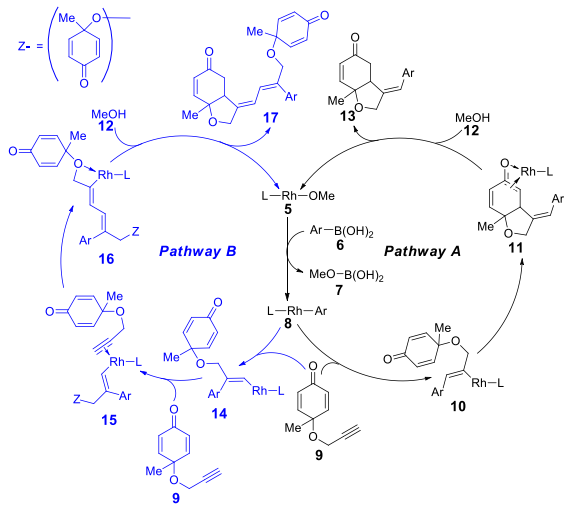


**Scheme 2** Proposed Catalytic Cycle for Rhodium-Catalyzed Synthesis of Hydrobenzofurans.

As shown in the mechanistic map[22] (Scheme 2), two possible pathways were taken into account. Both of the pathways begin with the transmetallation between methoxyrhodium complex **5** and aryl boronic acid **6** which generates the aryl-rhodium intermediate **8**. In pathway **A**, the *cis*- alkyne insertion of reactant **9** into rhodium–carbon bond affords intermediate **10**, in which the aryl group is linked with the terminal carbon of alkene group. Subsequent intramolecular alkene insertion gives complex **11**, followed by metholysis leads to the release of product **13**, as well as the regeneration of active catalyst **5**. The enantioselectivity is thought to be controlled by the intramolecular alkene insertion step. In pathway **B**, after the intramolecular alkyne insertion, rhodium is linked with the terminal alkynyl carbon. Following intermolecular alkyne insertion of another molecular reactant **9** forms complex **15**. Finally, the corresponding metholysis might give side product **17** and active catalyst **5**.

The rhodium catalyzed coupling reaction of cyclohexadienone-tethered alkyne with boronic acid **19** was chosen as the model reaction, and norbornadiene **L1** was chosen as the model ligand to theoretical study the mechanism of this type reaction (Scheme 3). Furthermore, (*R*)-BINAP **L2** and chiral bicyclo[2.2.2]octane type ligands **L3** and **L4** were employed to study the enantioselectivity of asymmetric desymmetrization step.

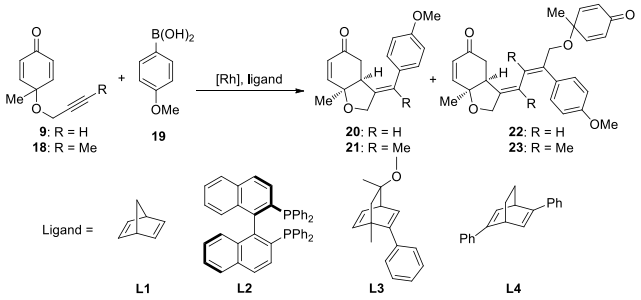


**Scheme 3** Model Reactions for the Mechanistic Investigation.

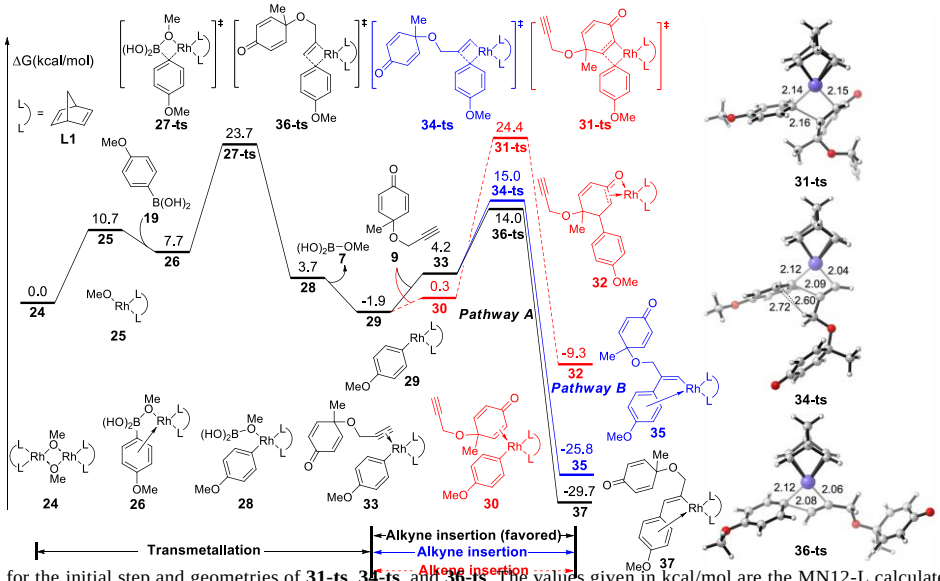


**Fig. 1** Free energy profile for the initial step and geometries of **31-ts**, **34-ts**, and **36-ts**. The values given in kcal/mol are the MN12-L calculated relative free energies in methanol solvent. The values of bond lengths are given in angstroms.

Free energy profile for the initial step is summarized in Figure 1. After dissociation of dimeric rhodium complex **24**, the monomeric rhodium complex **25** undergoes transmetallation with reactant **19** via a four-membered-ring transition state **27-ts**

with a barrier of 16.0 kcal/mol. The aryl-rhodium complex **29** is then generated with the release of methylborate. There are two reaction modes for the subsequent insertion of complex **9** into intermediate **29**. The reaction free energy of alkyne insertion from intermediate **29** to **37** via transition state **36-ts** is 15.9 kcal/mol. Following this pathway, major product **20** would be generated. In the other case, the insertion via transition state **34-ts** would irreversibly generates intermediate **35**, which is the precursor of side product **22**. The relative free energy of transition state **34-ts** is 1.0 kcal/mol higher than **36-ts** because of the steric repulsion between the substituted group of the alkyne and the aryl group (Figure 1). Therefore, pathway **A** is favourable comparing with pathway **B**, Which leads to the formation of major product **20**. This result is consistent with experimental observations. Besides, the alkene group insertion into aryl-rhodium via transition state **31-ts** was also calculated. The activation free energy is 26.3 kcal/mol, which is much higher than that of triple bond insertion transition states **34-ts** and **36-ts**.

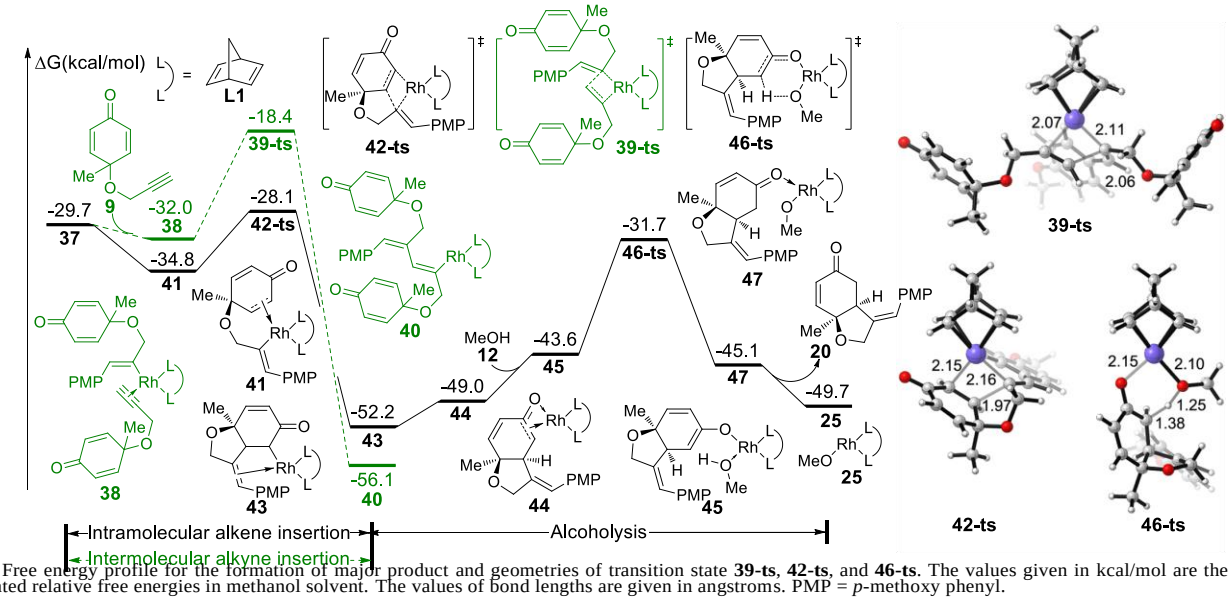


**Fig. 2** Free energy profile for the formation of major product and geometries of transition state **39-ts**, **42-ts**, and **46-ts**. The values given in kcal/mol are the MN12-L calculated relative free energies in methanol solvent. The values of bond lengths are given in angstroms. PMP = *p*-methoxy phenyl.

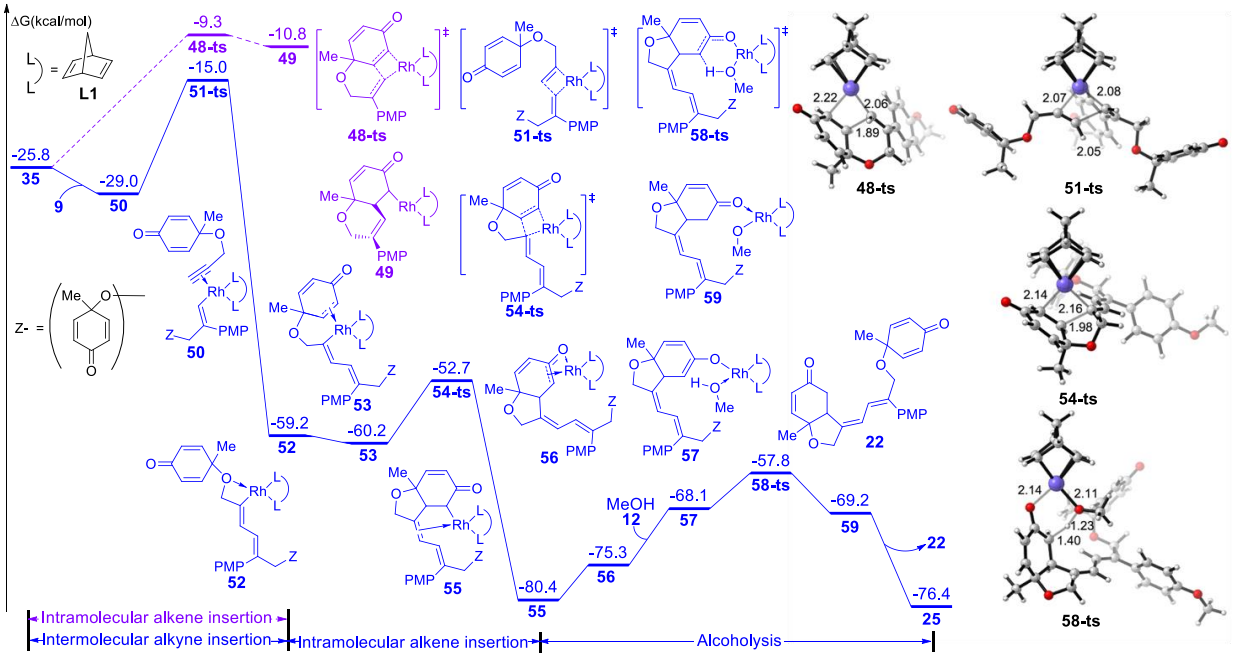


**Fig. 3** Free energy profile for the formation of side product and geometries of transition state **48-ts**, **51-ts**, **54-ts**, and **58-ts**. The values of bond lengths are given in angstroms. The values given in kcal/mol are the MN12-L calculated relative free energies in methanol solvent. PMP = *p*-methoxy phenyl.

As shown in Figure 2, intermediate **37** could isomerize to **41** through the coordination of intramolecular alkene to rhodium; this process is exothermic by 5.1 kcal/mol. Subsequently, intramolecular alkene insertion takes place via transition state **42-ts** (the geometry is shown in Figure 2) with only a barrier of 6.7 kcal/mol, and irreversibly generates intermediate **43**. When

intermediate **45** is formed with the coordination of methanol, the protonation of the carbon atom via transition state **46-ts** with a 20.5 kcal/mol energy barrier. After releasing product **20**, the active catalyst species **25** is regenerated to accomplish the catalytic cycle. The competition of intermolecular alkyne insertion has also been considered. When another molecular substrate **9** coordinates to intermediate **37**, the relative free energy decrease by 2.3 kcal/mol. Following alkyne insertion would occur via transition state **39-ts**, but the relative free energy for that transition state is 9.7 kcal/mol higher than that of transition state **42-ts**. Therefore, the insertion of another molecular alkyne is unfavorable.

On the other hand, free energy profile for the generation of side product **22** is summarized in Figure 3. When intermediate **35** is formed, intramolecular alkene insertion via transition state **48-ts** is inhibited because there is a *(Z)*- double bond in the six-membered-ring of insertion product **49**. Another molecular alkyne insertion could take place through transition state **51-ts**, generating the intermediate **52** with irreversibly. The isomerization from **52** to **53** is exothermic by 1.0 kcal/mol due to the coordination of the alkene group. The subsequent alkene insertion via transition state **54-ts** forms intermediate **55**. The coordination of methanol forms intermediate **57**. Then rhodium–carbon bond in intermediate **57** could be protonated by methanol via transition state **58-ts** with an overall activation free energy of 22.6 kcal/mol. After releasing one side product **22**, the active catalyst species **25** is regenerated.

**Table 1** Free energies of **27-ts**, **34-ts**, **36-ts** and **42-ts** with **L1**–**L4**

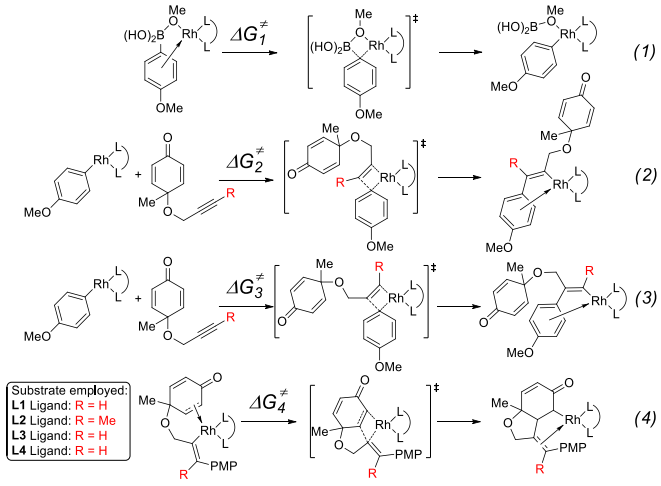


| entry | ligand | $\Delta G_1^{\neq}$ | $\Delta G_2^{\neq}$ | $\Delta G_3^{\neq}$ | $\Delta G_4^{\neq}$ |
|---|---|---|---|---|---|
| 1 | L1 | 16.0 | 15.9 | 16.9 | 6.7 |
| 2 | L2 | 14.8 | 13.5 | 18.3 | 5.5 |
| 3 | L3 | 14.5 | 12.8 | 14.8 | 5.7 |
| 4 | L4 | 15.1 | 9.0 | 12.6 | 5.6 |

The values of this Table are given in kcal/mol.

The mechanism and reactivity for rhodium-catalyzed synthesis of hydrobenzofurans with ligand **L2** was also studied. The activation free energies for the key steps are listed in Table 1 (the full potential energy surface for this reaction with ligand **L2** is given in Figure S1 in the Supporting Information). When the (*R*)-BINAP **L2** ligand is used, the activation free energy ($\Delta G_2^{\neq}$) of the insertion step (eq 2) is 13.5 kcal/mol. The activation energy ($\Delta G_3^{\neq}$) with ligand **L2** of the insertion (eq 3) leading to the side product is 18.3 kcal/mol, which is 4.8kcal/mol higher than that of the insertion (eq 2) leading to the major product. Theoretical results indicate that compared with ligand **L1**, less side product would be obtained when ligand **L2** is used. The activation free energy ($\Delta G_4^{\neq}$) for intramolecular alkene insertion (eq 4) with ligand **L2** is 5.5 kcal/mol, which is 1.2 kcal/mol lower than that with ligand **L1**. The reactivities of these key steps with ligands **L3** and **L4** are also listed in Table 1.[23]

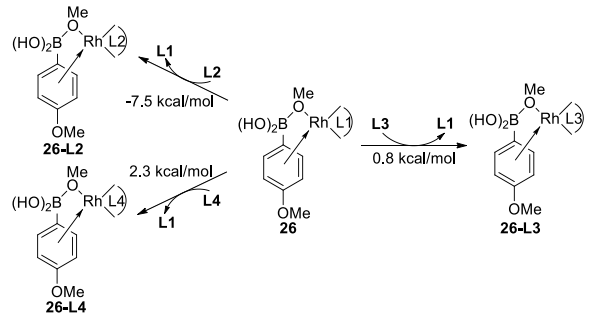


**Fig. 4** Ligand exchange energies of intermediate **26** for ligands **L2**–**L4**. The values are Gibbs free energy.

The experimental results indicate that when ligand **L1**, **L2**, or **L3** is used, a high yield of major product is obtained. However, a very low yield of product is obtained when ligand **L4** is used. This result conflicts with the calculated energy profiles (Table 1 and Figures S1, S3, and S5). Therefore, the binding energies of ligands **L1**–**L4** were calculated to understand the different reactivity. As shown in Figure 4, intermediate **26** was chosen as the model to study the binding energy of ligands. The binding energy of the (*R*)-BINAP ligand **L2** is 7.5 kcal/mol higher than ligand **L1**, when intermediate **26-L2** is formed. The ligand exchange energy with ligand **L3** is 0.8 kcal/mol, which indicates that the binding of ligand **L3** is weaker than that of ligand **L2**. The ligand exchange energies with ligand **L4** are 2.3 kcal/mol. Therefore, the lower binding energies of ligands **L4** result in the lower yield of major product.

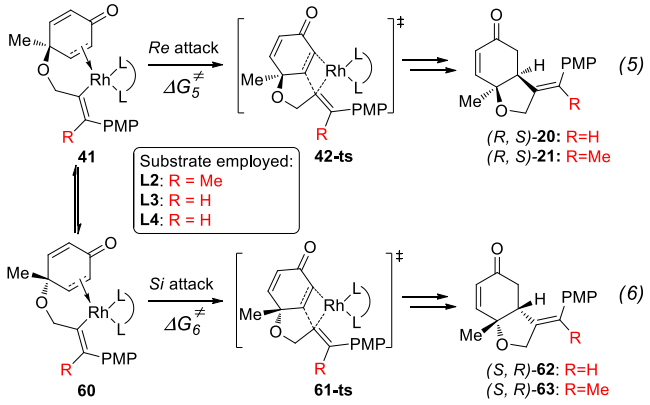


**Fig. 5** Enantioselectivity determining step for the desymmetrization of cyclohexadienone.

As shown in Figure 5, the enantioselectivity for the desymmetrization of cyclohexadienone is controlled by the free energy difference between the irreversible intramolecular alkene insertion steps via the four-membered-ring transition state **42-ts** or **61-ts**. The *Re*-face attack (via transition state **42-ts**) would lead to the (*4R, 5S*)-cyclohexaenone product, while the (*4S, 5R*)-cyclohexaenone product would be generated by *Si*-face attack via transition state **61-ts**.

**Table 2** Calculated *ee* Values at 300 K and Experimentally Observed *ee* Values with Ligand **L2**–**L4**

| entry | ligand | $\Delta\Delta G^{\neq} = (\Delta G_6^{\neq} - \Delta G_5^{\neq})$ | ee (calc.) | ee (exp.) |
|---|---|---|---|---|
| 1 | L2 | 2.3 | 96% | 96% |
| 2 | L3 | 2.7 | 98% | 76% |
| 3 | L4 | -0.2 | -17% | -6% |

Based on these results, the ee values were predict from Eyring equation (eq 7), where *R* is the gas constant, T is absolute temperature, *k* is reaction rate constant. The calculated *ee* value is derived from this equation at 300 K in methanol.

$$ee = (k_S/k_R\text{-}1)/(k_S/k_R\text{+}1) = (e^{\Delta\Delta G^{\neq}/RT}\text{-}1)/(e^{\Delta\Delta G^{\neq}/RT}\text{+}1) \quad (7)$$

The theoretically calculated and experimentally observed *ee* values[11,12] with ligands **L2**–**L4** are shown in Table 2.[24] When ligand **L2** is used, the calculated *ee* is 96%, which is consistent with experimental observation. The enantioselectivity is determined by the energy difference between transition states **42-ts-L2** and **61-ts-L2** (Figure 6). The closest H...H distance is 2.29 Å in transition state **61-ts-L2**. This result indicates that the steric repulsion between the aryl moiety of the substrate and the phenyl group of the ligand leads to the relative free energy of **61-ts-L2** 2.3 kcal/mol higher than that of **42-ts-L2**. When ligand **L3** is used, the calculated *ee* value is 22% higher than the experimental observed value. In the geometry of **61-ts-L3**, the closest distance between the oxygen atom in the carbonyl group of the substrate and a carbon atom in the phenyl group of ligand is 3.39 Å. Thus, the higher relative free energy of **61-ts-L3** can be attributed to the steric repulsion between the carbonyl group of the substrate and the phenyl group of the ligand. When ligand **L4** is used, the calculated *ee* value is -17%, which is close to experimental observation. In the geometry of **42-ts-L4**, the C...O distance between the oxygen atom in the carbonyl group of the substrate and carbon atoms in the phenyl group of ligand are 3.16 Å and 3.25 Å, but the distance between phenyl group of ligand and 4-methoxyphenyl group of substrate is 3.38 Å. Therefore, the low enantioselectivity can be attributed to an attractive, none-noncovalent interaction between the phenyl group of ligand and *p*-methoxy phenyl group of substrate.

To better illustrate the steric repulsions at different regions of the ligand, 2D contour maps along the z axis of the van der Waals surface[25] of **L2-Rh**, **L3-Rh** and **L4-Rh** are plotted in Figure 7. The geometries of **L2-Rh**, **L3-Rh** and **L4-Rh** are respectively derived from transition state structure of **61-ts-L2, 61-ts-L3** and **42-ts-L4** through omitting the substrates.

When ligand **L2** is used, the atoms closest to the substrates, which result in the most steric repulsion, are two of the standing phenyl groups (labeled in red). This highly hindered region is very close to the phenyl group on the substrate of **61-ts-L2** (labeled by "X" in Figure 7a). Similarly, the strong stereogenic control by ligand **L3**, **L4** can be attributed to the repulsion between the phenyl group on ligand and the substrate (labeled by "X" in Figure 7b and 7c). These figures provide a straightforward explanation for the enantioselectivities observed in the asymmetric synthesis of hydrobenzofurans by rhodium-catalyzed cyclohexadienone reaction.

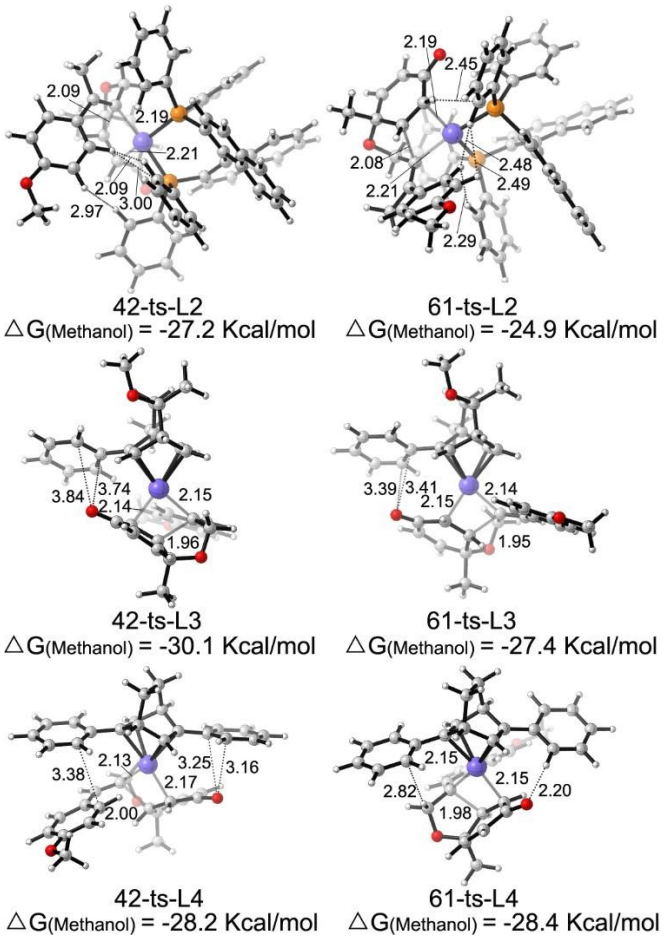


**Fig. 6** Geometries of transition state **42-ts** and **61-ts** with **L2**, **L3** and **L4** ligand. The values of bond lengths are given in angstroms. The values given in kcal/mol are the MN12-L calculated relative free energies.

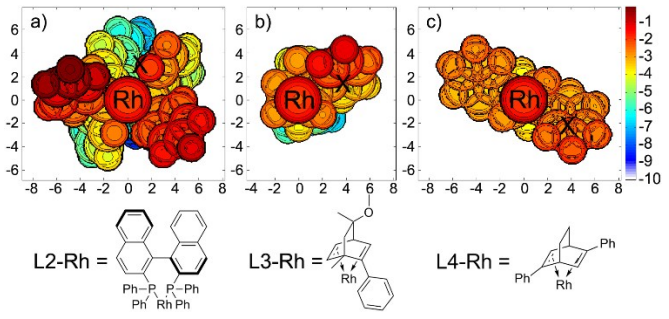

**Fig. 7** 2D contour maps of the van der Waals surface of ligands **L2**, **L3** and **L4** with rhodium. Distances are valued in Å. Rh is located at the origin of the coordinate system in the contour maps. Contour line of zero is defined as in the same plane of the Rh atom. Negative distance (blue) indicates the atoms on ligand is farther away from substrate; positive distance (red) indicates the atoms on ligand is closer to substrate.

## Conclusions

The newly reported density functional theory method MN12-L was employed to clarify the mechanism, reactivity, and enantioselectivity for the asymmetric synthesis of hydrobenzofurans through rhodium-catalyzed desymmetrization of cyclohexadienone reaction. The reaction pathway involves the transmetallation of aryl boronic acid to form an aryl-rhodium compound, intermolecular alkyne insertion, intramolecular olefin insertion, and protonation to generate the hydrobenzofurans product. Another type of intermolecular alkyne insertion would lead to the generation of a side product, which is in competition with the major pathway. The addition of biphosphine- and diene-type ligands results in similar reactivity as the corresponding activation energies of the key steps are close. However, the bulky diene-type ligands give very low yield and enantioselectivity, which can be attributed to the low binding energies. Moreover, the calculated enantioselectivity, which corresponds well with the experimental observations, can be explained by the steric repulsion between substrate and ligand.

## Acknowledgements

We thank Professor Stephen G. Newman of University of Ottawa, Professor Mark Lautens and Doctor Juliane Keilitz of University of Toronto for helpful discussions. This work was supported by the National Natural Science Foundation of China (Grants 51302327 and 21372266), and the Foundation of 100Yong Chongqing University (Project 0903005203191). We are also thankful for the project (No.106112015CDJZR228806) supported by the Fundamental Research Funds for the Central Universities (Chongqing University). This work was supported by the China Scholarship Council.

## Notes and references

1 (a) Y.-Q. Chen, Y.-H. Shen, Y.-Q. Su, L.-Y. Kong and W.-D. Zhang, *Chem. Biodiversity*, 2009, **6**, 779–783. (b) P. D. Brown, A. C. Willis, M. S. Sherburn and A. L. Lawrence, *Org. Lett*., 2012, **14**, 4537–4539. (c) K. Zhao, G.-J. Cheng, H. Yang, H. Shang, X. Zhang, Y.-D. Wu and Y. Tang, *Org. Lett*., 2012, **14**, 4878–4881. (d) J. Tian, Q.-S. Zhao, H.-J. Zhang, Z.-W. Lin and H.-D. Sun, *J. Nat. Prod.*, 1997, **60**, 766–769. (e) Y.-P. Gao, Y.-H. Shen, S.-D. Zhang, J.-M. Tian, H.-W. Zeng, J. Ye, H.-L. Li, L. Shan and W.-D. Zhang, *Org. Lett*., 2012, **14**, 1954–1957. (f) J. K. Hexum, R. Tello-Aburto, N. B. Struntz, A. M. Harned and D. A. Harki, *ACS Med. Chem. Lett*., 2012, **3**, 459–464.

2 (a) X. Yang, J. Wang and P. Li, *Org. Biomol. Chem.*, 2014, **12**, 2499–2513. (b) N. Miyamae, N. Watanabe, M. Moritaka, K. Nakano, Y. Ichikawa and H. Kotsuki, *Org. Biomol. Chem.*, 2014, **12**, 5847–5855. (c) Q. Gu and S.-L. You, *Org. Lett*., 2011, **13**, 5192–5195. (d) H. U. Vora and T. Rovis, *Aldrichimica Acta*., 2011, **44**, 3–11. (e) Q. Gu and S.-L. You, *Chemical Science*., 2011, **2**, 1519–1522.

3 (a) X. Su, W. Zhou, Y. Li and J. Zhang, *Angew. Chem., Int. Ed*., 2015, **54**, 6874–6877. (b) S. Takizawa. T. M.-N. Nguyen, A. Grossmann, D. Enders and H. Sasai, *Angew. Chem., Int. Ed*., 2012, **51**, 5423–5426.

4 (a) R. Kuniyil and R. B. Sunoj, *Org. Lett*., 2013, **15**, 5040–5043. (b) M.-Q. Jia, C. Liu and S.-L. You, *J. Org. Chem*., 2012, **77**, 10996–11001. (c) N. E. Wurz, C. G. Daniliuc and F. Glorius, *Chem.–Eur. J*., 2012, **18**, 16297–16301. (d) A. Bhunia, S. R. Yetra, S. S. Bhojgude and A. T. Biju, *Org. Lett*., 2012, **14**, 2830–2833. (e) M.-Q. Jia and S.-L. You, *Chem. Commun*., 2012, **48**, 6363–6365. (f) Q. Liu and T. Rovis, *J. Am. Chem. Soc*., 2006, **128**, 2552–2553. (g) Q. Liu and T. Rovis, *Org. Process Res. Dev*., 2007, **11**, 598–604.

5 For reviews, see: (a) X.-F. Wu, H. Neumann and M. Beller, *chem. Soc. Rev*., 2011, **40**, 4986–5009. (b) E.-i. Negishi, C. Copéret, S. Ma, S.-Y. Liou and F. Liu, *Chem. Rev*., 1996, **96**, 365–393. (c) B. E. Rossiter and N. M. Swingle, *Chem. Rev*., 1992, **92**, 771–806. (d) K. A. Kalstabakken and A. M. Harned, *Tetrahedron.*, 2014, **70**, 9571–9585. (e) A. Marinetti; H. Jullien and A. Voituriez, *Chem. Soc. Rev*., 2012, **41**, 4884–4908. (f) L. F. Tietze, *Chem. Rev*., 1996, **96**, 115–136.

6 As recent examples of transition-metal catalyzed desymmetrization of cyclohexadienones reactions, see: (a) P. Liu, Y. Fukui, P. Tian, Z.-T. He, C.-Y. Sun, N.-Y. Wu and G.-Q. Lin, *J. Am. Chem. Soc*., 2013, **135**, 11700–11703. (b) R. Tello-Aburto and A. M. Harned, *Org. Lett*., 2009, **11**, 3998–4000. (c) S. Cai, Z. Liu, W. Zhang, X. Zhao and D. Z. Wang, *Angew. Chem., Int. Ed*., 2011, **50**, 11133–11137. (d) R. Imbos, M. H. G. Brilman, M. Pineschi and B. L. Feringa, *Org. Lett.*, 1999, **1**, 623–625. (e) K. Takenaka, S. C. Mohanta and H. Sasai, *Angew. Chem., Int. Ed*., 2014, **53**, 4675–4679.

7 (a) T. Hayashi and K. Yamasaki, *Chem. Rev*., 2003, **103**, 2829–2844. (b) H. J. Edwards, J. D. Hargrave, S. D. Penrose and C. G. Frost, *Chem. Soc. Rev*., 2010, **39**, 2093–2105. (c) G. P. Howell, *Org. Process Res. Dev.*, 2012, **16**, 1258–1272. (d) Z.-Q. Wang, C.-G. Feng, M.-H. Xu and G.-Q. Lin, *J. Am. Chem. Soc*., 2007, **129**, 5336–5337. (e) E. Okazaki, R. Okamoto, Y. Shibata, K. Noguchi and K. Tanaka. *Angew. Chem., Int. Ed*., 2012, **51**, 6722–6727. (f) T. A. Davis, T. K. Hyster, T. Rovis, *Angew. Chem., Int. Ed*., 2013, **52**, 14181–14185. (g) R. Shintani, W.-L. Duan and T. Hayashi, *J. Am. Chem. Soc*., 2006, **128**, 5628–5629. (h) T. Seiser and N. Cramer, *Chem.–Eur. J*., 2010, **16**, 3383–3391. (i) Y. Takaya, M. Ogasawara and T. Hayashi, *J. Am. Chem. Soc*., 1998, **120**, 5579–5580.

8 (a) S. Gosiewska, J. A. Raskatov, R. Shintani, T. Hayashi and J. M. Brown, *Chem.–Eur. J.*, 2012, **18**, 80–84. (b) D. A. DiRocco, E. L. Noey, K. N. Houk, T. Rovis, *Angew. Chem., Int. Ed*., 2012, **51**, 2391–2394. (c) C. Shao, H.-J. Yu, N.-Y. Wu, C.-G. Feng and G.-Q. Lin, *Org. Lett*., 2010, **12**, 3820–3823. (d) R. Tello-Aburto, K. A. Kalstabakken, K. A. Volp and A. M. Harned, Org. Biomol. Chem., 2011, 9, 7849–7859. (e) Y. Li and M.-H. Xu, *Org. Lett*., 2014, **16**, 2712–2715.

9 (a) H.-L. Qin, J.-B. Han, J.-H. Hao and E. A. B. Kantchev, *Green Chem*., 2014, **16**, 3224–3229. (b) L. R. Domingo, R. J. Zaragozá, J. A. Saéz and M. Arnó, *Molecules*., 2012, **17**, 1335–1353. (c) E. A. B. Kantchev, S. R. Pangestu, F. Zhou, M. B. Sullivan and H.-B. Su, *Chem.–Eur. J.*, 2014, **20**, 15625–15634. (d) K. Sasaki, T. Nishimura, R. Shintani, E. A. B. Kantchev and T. Hayashi, *Chem. Sci*., 2012, **3**, 1278–1283. (e) E. A. B. Kantchev, *Chem. Sci*., 2013, **4**, 1864–1875. (f) E. A. B. Kantchev, *Chem. Commun*., 2011, **47**, 10969–10971. (g) S. Liu, H. Shen, Z. Yu, L. Shi, Z. Yang, Y. Lan, *Organometallics*., 2014, **33**, 6282–6285.

10 (a) P. Tian, H.-Q. Dong and G.-Q. Lin, *ACS Catal*., 2012, **2**, 95–119. (b) Y. Fukui, P. Liu, Q. Liu, Z.-T. He, N.-Y. Wu, P.

Tian and G.-Q. Lin, *J. Am. Chem. Soc*., 2014, **136**, 15607–15614.
11 J. Keilitz, S. G. Newman and M. Lautens, *Org. Lett*., 2013, **15**, 1148–1151.
12 Z.-T. He, B. Tian, Y. Fukui, X. Tong, P. Tian and G.-Q. Lin, *Angew. Chem., Int. Ed*., 2013, **52**, 5314–5318.
13 (a) R. Noyori, *Acc. Chem. Res*., 1990, **23**, 345–350. (b) M. Kitamura, M. Tsukamoto, Y. Bessho, M. Yoshimura, U. Kobs, M. Widhalm and R. Noyori, *J. Am. Chem. Soc.*, 2002, **124**, 6649–6667. (c) C. A. Sandoval, T. Ohkuma, K. Muñiz and R. Noyori, *J. Am. Chem. Soc.*, 2003, **125**, 13490–13503. (d) R. Kramer and R. Brückner, *Angew. Chem., Int. Ed*., 2007, **46**, 6537–6541. (e) T. Hayashi, M. Takahashi, Y. Takaya and M. Ogasawara *J. Am. Chem. Soc*., 2002, **124**, 5052–5058. (f) S.-Y. Wang, S.-J. Ji and T.-P. Loh, *J. Am. Chem. Soc.*, 2007, **129**, 276–277. (g) D. A. Evans and R. J. Thomson, *J. Am. Chem. Soc.*, 2005, **127**, 10506–10507. (h) S. Ge and J. F. Hartwig, *J. Am. Chem. Soc.*, 2011, **133**, 16330–16333.
14 M. J. Frisch, G. W. Trucks, H. B. Schlegel, G. E. Scuseria, M. A. Robb, J. R. Cheeseman, G. Scalmani, V. Barone, B. Mennucci, G. A. Petersson, H. Nakatsuji, M. Caricato, X. Li, H. P. Hratchian, A. F. Izmaylov, J. Bloino, G. Zheng, J. L. Sonnenberg, M. Hada, M. Ehara, K. Toyota, R. Fukuda, J. Hasegawa, M. Ishida, T. Nakajima, Y. Honda, O. Kitao, H. Nakai, T. Vreven, J. A. Montgomery, Jr., J. E. Peralta, F. Ogliaro, M. Bearpark, J. J. Heyd, E. Brothers, K. N. Kudin, V. N. Staroverov, T. Keith, R. Kobayashi, J. Normand, K. Raghavachari, A. Rendell, J. C. Burant, S. S. Iyengar, J. Tomasi, M. Cossi, N. Rega, J. M. Millam, M. Klene, J. E. Knox, J. B. Cross, V. Bakken, C. Adamo, J. Jaramillo, R. Gomperts, R. E. Stratmann, O. Yazyev, A. J. Austin, R. Cammi, C. Pomelli, J. W. Ochterski, R. L. Martin, K. Morokuma, V. G. Zakrzewski, G. A. Voth, P. Salvador, J. J. Dannenberg, S. Dapprich, A. D. Daniels, Ö. Farkas, J. B. Foresman, J. V. Ortiz, J. Cioslowski, and D. J. Fox, *Gaussian 09, Revision D. 01*, 2013, **Gaussian, Inc**., Wallingford CT.
15 (a) A. D. Becke, *J. Chem. Phys.*, 1993, **98**, 5648–5652. (b) C. Lee, W. Yang and R. G. Parr, *Phys. Rev. B: Condens. Matter Mater. Phys.*, 1988, **37**, 785–789. (c) P. J. Stephens, F. J. Devlin, C. F. Chabalowski and M. J. Frish, *J. Phys. Chem.*, 1994, **98**, 11623–11627.
16 (a) P. C. Hariharan and J. A. Pople, *Theoret. Chimica Acta*., 1973, **28**, 213–222. (b) W. J. Hehre, R. Ditchfield and J. A. Pople, *J. Chem. Phys*., 1972, **56**, 2257–2261. (c) J. D. Dill and J. A. Pople, *J. Chem. Phys*., 1975, **62**, 2921–2923. (d) M. M. Francl, W. J. Pietro, W. J. Hehre, J. S. Binkley, M. S. Gordon, D. J. Defrees and J. A. Pople, *J. Chem. Phys*., 1982, **77**, 3654–3665.
17 (a) P. J. Hay and W. R. Wadt, *J. Chem. Phys.*, 1985, **82**, 270–283. (b) W. R. Wadt and P. J. Hay, *J. Chem. Phys.*, 1985, **82**, 284–298. (c) P. J. Hay and W. R. Wadt, *J. Chem. Phys*., 1985, **82**, 299–310.
18 (a) R. Peverati and D. G. Truhlar, *Phys. Chem. Chem. Phys*., 2012, **14**, 13171–13174. (b) M. Hölscher and W. Leitner, *Eur. J. Inorg. Chem*., 2014, 6126–6133.
19 (a) A. V. Marenich, C. J. Cramer and D. G. Truhlar, *J. Phys. Chem. B*, 2009, **113**, 6378–6396. (b) A. V. Marenich, C. J. Cramer and D. G. Truhlar, *J. Phys. Chem. B*, 2009, **113**, 4538–4543. (c) X. Xu, P. Liu, X.-Z. Shu, W. Tang, K. N. Houk, *J. Am. Chem. Soc*., 2013, **135**, 9271–9274.
20 (a) R. Krishnan, J. S. Binkley, R. Seeger and J. A. Pople, *J. Chem. Phys.*, 1980, **72**, 650–654. (b) A. D. McLean and G. S. Chandler, *J. Chem. Phys.*, 1980, **72**, 5639–5648.
21 L. E. Roy, P. J. Hay and R. L. Martin, *J. Chem. Theory Comput*., 2008, **4**, 1029–1031
22 (a) K. Fagnou and M. Lautens, *Chem. Rev*., 2003, **103**, 169–196. (b)Z. Yu and Y. Lan, *J. Org. Chem.*, 2013, **78**, 11501–11507.
23 The full potential energy surfaces for this reaction with ligands **L2**, **L3**, and **L4** are given in Figures S1, S3, and S5, respectively, in the Supporting Information.
24 The B97D3 functional, M06-L functional and M11-L functional calculated *ee* values are given in Table S1, in the Supporting Information.
25 (a) S. S. Batsanov, *Inorg. Mater*., 2001, **37**, 871–885. (b) P. Liu, J. Montgomery and K. N. Houk, *J. Am. Chem. Soc*., 2011, **133**, 6956–6959. (c) A. Poater, F. Ragone, R. Mariz, R. Dorta and L. Cavallo, *Chem.–Eur. J*., 2010, **16**, 14348–14353. (d) F. Ragone, A. Poater and L. Cavallo, *J. Am. Chem. Soc.*, 2010, **132**, 4249–4258. (e) X. Hong, P. Liu and K. N. Houk, *J. Am. Chem. Soc*., 2013, **135**, 1456–1462. (f) H. Wang, P. Kohler, L. E. Overman, K. N. Houk, *J. Am. Chem. Soc.*, 2012, **134**, 16054–16058.